Available online at www.sciencedirect.com
ScienceDirect
Polymer 47 (2006) 7271–7281
polymer
www.elsevier.com/locate/polymer

Effects of shear flow on a semidilute polymer solution under phase-separating condition

Maya K. Endoh [a,1], Mikihito Takenaka [a], Takeji Hashimoto [a,b,*]

[a] Department of Polymer Chemistry, Graduate School of Engineering, Kyoto University, Katsura, Kyoto 615-8510, Japan
[b] Advanced Science Research Center, Japan Atomic Energy Agency, Tokai-mura, Ibaraki 819-1195, Japan

Received 13 February 2006; received in revised form 23 May 2006; accepted 24 May 2006
Available online 7 July 2006

Abstract

We studied the effects of a step-up shear flow from zero shear rate to the given shear rate, $\dot{\gamma}$, on formation of shear-induced structures for a semidilute polystyrene (PS)/diethyl malonate (DEM) solution below its cloud point temperature where the solution undergoes phase separation via spinodal decomposition (SD) in quiescent state. We elucidated that the effects of step-up shear can be divided into two regions: below and above a critical shear rate, $\dot{\gamma}_{c,SD}$. At $\dot{\gamma} < \dot{\gamma}_{c,SD}$, growing phase-separated domains via SD are found to be deformed under the flow, so that FFT spectra of the shear-microscopy images become elliptical with the wave number q_{mx} at the maximum intensity parallel to the flow being smaller than the corresponding wave number q_{mz} parallel to the neutral axis. However, strikingly enough, the aspect ratio q_{mz}/q_{mx} of the elliptic spinodal ring observed for this system was much smaller than that observed for binary fluids. The unique feature was proposed to be the elastic effect inherent in this system. When $\dot{\gamma}$ is larger than $\dot{\gamma}_{c,SD}$, however, initially phase-separating structures via SD are strongly deformed and distorted. Interestingly enough, the light scattering pattern was transformed from the isotropic ring pattern into the butterfly pattern. This is interpreted as follows: when $\dot{\gamma} > \dot{\gamma}_{c,SD}$, there may not be enough time for the domains composed of elastically deformed swollen-network chains to relax, and consequently the domains are cooperatively disrupted. The disrupted domains tend to squeeze solvent in order to release the elastic free energy stored in the deformed swollen-network chains, resulting in anisotropic domain more extended to neutral axis than flow direction and hence giving rise to the butterfly pattern.

Keywords: Phase-separation; Semidilute solution; Butterfly pattern

1. Introduction

In the last three decades, the shear-induced concentration fluctuations and/or phase separation have been extensively investigated for thermodynamically stable, single-phase, and semidilute polymer solutions in quiescent state [1–7]. However, there are no experimental studies on the effects of a shear flow on the phase-separation processes of semidilute polymer solutions in two-phase region at quiescent state, although there are some reports concerning two-dimensional (2D) computer simulations [8]. Therefore, in this paper, we shall present our works that challenged to study how the shear flow affects the phase-separating structure in semidilute polymer solutions. This may further enrich our knowledge concerning the formation of dissipative structure (ordered structures developed in open nonequilibrium systems) in the thermodynamically unstable state as well as the stable state. For this purpose, we first quenched our system into the thermodynamically unstable state to develop the isotropic phase-separating structure via spinodal decomposition (SD) in a quiescent solution, and then imposed the step-up shear flow to the same system which has the as-developed SD structure. We investigated the time changes in the phase-separating structure after the onset of the step-up shear flow as a function of shear rate.

* Corresponding author at: Advanced Science Research Center, Japan Atomic Energy Agency, Tokai-mura, Ibaraki 819-1195, Japan.
E-mail addresses: hashimoto.takeji@jaea.go.jp, hashi2@pearl.ocn.ne.jp (T. Hashimoto).
[1] Present address: 31 Perigee Dr., Stony Brook, NY 11790, USA.

0032-3861/$ - see front matter © 2006 Elsevier Ltd. All rights reserved.
doi:10.1016/j.polymer.2006.05.075

Before going into detailed discussion, we shall first describe the background of present work.

If the dynamical properties of each component in binary mixtures, such as viscosity and self-diffusion coefficient, are symmetric, the shear-induced mixing and/or homogenization occurs for the systems in thermodynamically unstable state or two-phase region, provided that the segregation power or interfacial tension is sufficiently small compared to the mechanical energy imposed to the systems [9–17]. The shear-induced homogenization or single-phase formation is clearly demonstrated by a distinct difference in the scaled structure factors before and after the homogenization [9,14]. Theoretically, the dynamics of concentration fluctuations of dynamically symmetric binary fluids, such as simple liquid mixtures and polymer blends, is expressed by so-called model H [18] which includes the effects of the hydrodynamic interactions. The model H predicts that the hydrodynamic interactions shift downward the critical temperature as also suggested by Onuki [17].

On the other hand, if the systems are dynamically asymmetric, such as semidilute solutions of high molecular weight polymers and polymer mixtures having a large difference in molecular weights [3–7,9,17,19–21] or glass transition temperature, T_g [22], the shear-induced concentration fluctuations and/or phase separation occur even in the case of thermodynamically stable state or one-phase region. We have explained this phenomenon by the solvent squeeze mediated by the elastic effects [6,7,20,21]. In quiescent semidilute polymer solutions, there are thermal concentration fluctuations, giving rise to regions of higher and lower polymer concentrations which have higher and lower number densities of entanglement couplings, respectively. The stress built-up in the systems is borne only by the slow component, which is a polymer, because solvent (the fast component) relaxes much faster than polymer. As a result, stress imbalance arises [23–26]. When the shear flow is imposed on such systems, the stress borne by polymers tends to become higher in the more entangled regions due to the concentration dependence of the viscosity and the normal stress coefficients. The stress or the elastic free energy stored in the solutions by deformation of the swollen entangled polymer chains is relaxed by disentanglements, when the shear rate, $\dot{\gamma}$, is smaller than the terminal relaxation rate, τ_w^{-1}, of the solution. However, when $\dot{\gamma}$ is higher than τ_w^{-1}, the elastic free energy is released only by squeezing of solvent: squeezing of solvent can relax conformation of the deformed swollen entangled chains and hence stored elastic energy. The higher the concentration is, the larger the stored elastic free energy is, and therefore the more the solvent is squeezed. As a result, concentration fluctuations are built up under the shear flow against the osmotic pressure.

The theoretical framework for the dynamically asymmetric systems is proposed by Helfand and Fredrickson [23], Milner [24], and Onuki [25,26] (HFMO). The HFMO theory takes into account the dynamical coupling between stress and diffusion. This coupling becomes dramatically remarkable when the constituents of a mixture have a very large dynamical asymmetry. According to the theory, the dynamics of concentration fluctuations is described by the following generalized time-dependent Ginzburg–Landau (TDGL) type equation where the coupling between stress and diffusion is incorporated in the second term of the bracket in right hand side (rhs) of the equation below,

$$\left(\frac{\partial}{\partial t}+\mathbf{v}\times\nabla\right)\phi=\nabla\times L\left[\nabla\frac{\delta F}{\delta\phi}-\alpha\nabla\times\sigma^{(n)}\right]+\left(\text{H.D. term}\right)+\theta_\phi \tag{1}$$

where $\mathbf{v}$ is the volume average velocity, ϕ the volume fraction of polymer, L the Onsager kinetic coefficient, F the free energy functional, $\sigma^{(n)}$ the stress tensor of the polymer under a flow, H.D. term the hydrodynamic interaction term [27], and θ_ϕ is the thermal noise term. Here α is the dynamical asymmetry parameter.

In the case of dynamically symmetric systems, α becomes zero, so that Eq. (1) reduces to model H [18]. However, α is not zero for dynamically asymmetric systems and becomes $\alpha \cong 1/\phi$ for polymer solutions. When such systems in a thermodynamically single-phase state are brought under the shear flow, the stress term produces the instability of concentration fluctuations [28]. Therefore the shear-induced concentration fluctuations and/or phase separation occurs, even though the systems are in one-phase region at quiescent state.

When the solutions are subjected to a shear flow in the thermodynamically unstable region at quiescent state, the term associated with the thermodynamic force (''*the first term*'' in the square bracket of rhs of Eq. (1)), the hydrodynamic interaction term, and the noise term, θ_ϕ, as well as the stress term (''*the second term*'' in the square bracket of rhs of Eq. (1)) enhance the concentration fluctuations. On the other hand, the stress term is the only trigger to enhance the concentration fluctuations when the solutions are in a thermodynamically stable state at quiescent state.

We expect that the second term becomes significantly important relative to the first term for the formation of shear-induced structures with increasing $\dot{\gamma}$. Thus we anticipate that there may be a critical shear rate, defined hereafter as $\dot{\gamma}_{c,SD}$, above which the second term dominates the first term; $\dot{\gamma}_{c,SD}$ is defined as the critical shear rate, when the system is in the spinodal region in the phase diagram. We aim to investigate whether there are some dramatic differences in the shear-induced structures below and above $\dot{\gamma}_{c,SD}$. $\dot{\gamma}_{c,SD}$ should formally correspond to the critical shear rate, $\dot{\gamma}_c$, in the thermodynamically stable solutions where the second term for enhancing concentration fluctuations outweighs the first term for decaying concentration fluctuations.

2. Experimental methods

2.1. Materials

The system studied is polystyrene (PS) dissolved in diethyl malonate (DEM). The weight-average molecular weight, M_w, of PS is 5.48×10^6, and the heterogeneity index for the

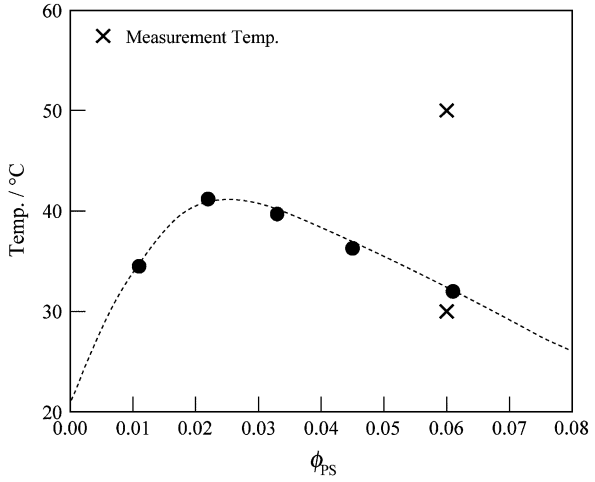

Fig. 1. Cloud point curve of the PS/DEM solution. Filled circles denote the cloud point, and crosses denote the temperature and concentration at which the light scattering experiments and the microscope observations were carried out. The dotted line is a visual guide.

molecular weight distribution, M_w/M_n (M_n: number-average molecular weight) is 1.15. The concentration of PS, c, prepared was 6.0 wt.%. The c/c^* value is about 7 for this system at 27 °C, where the c^* is the overlap concentration described in the previous paper [7]. The solution has the Θ temperature of 35 °C and the cloud point, T_{cl}, 32 °C in quiescent state. It has an upper-critical-solution-temperature (UCST) type phase diagram as shown in Fig. 1.

2.2. Light scattering and optical microscopy

Small-angle light scattering (SALS) experiment under the continuous shear flow was carried out with a flow-SALS apparatus [29]. The two-dimensional (2D) SALS patterns on a screen, placed as shown in Fig. 2(a), were captured by a CCD camera. An He–Ne laser having a wavelength of 632.8 nm was used as an incident beam source. We detected the scattering patterns in the q_x–q_z plane by using a transparent cone-and-plate type shear cell made of quartz with 80 mm diameter and 1° cone angle. Here q is the magnitude of the scattering vector, **q**, and x, y, and z axes are taken parallel to the flow direction, the velocity gradient direction, and the neutral direction, respectively. q_x, q_y and q_z are the respective components of **q**. The schematic diagram of the apparatus is shown in Fig. 2(a) together with the optical set-up, and the coordinate system. Fig. 2(b) demonstrates one of the typical SALS pattern developed for the same solution chosen in present study after the onset of the shear flow above $\dot{\gamma}_c$ at 50 °C which is above T_{cl} in quiescent state. This anisotropic pattern is so-called "*butterfly*" pattern [4,5], reflecting shear-enhanced concentration fluctuations induced in the single-phase solution. The figure also defines the azimuthal angle, μ, for the scattering pattern. We measured *in situ* and at *real time* changes in the real space images, too, under an optical microscopy with a halogen lamp as a light source [29], though Fig. 2(a) does not show this part.

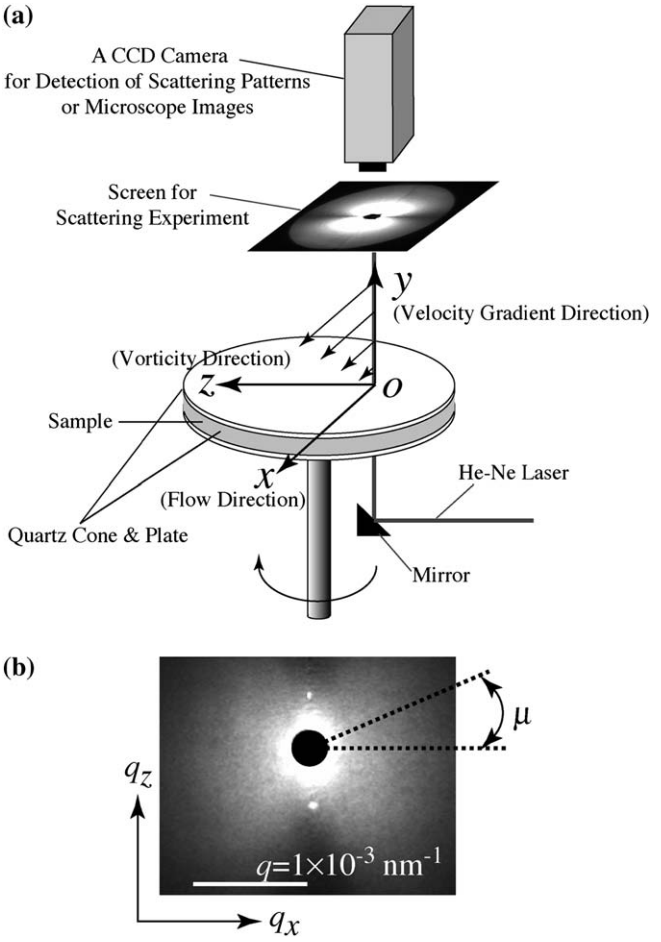

Fig. 2. (a) Schematic diagram of the shear-SALS set-up and definition of Cartesian coordinate. The x axis is parallel to the flow direction, the y axis to the shear gradient direction, and the z axis to the vorticity or neutral direction. The propagation of the incident beam is along the y axis, and light scattering intensity distribution is recorded in the q_x–q_z plane. Here q is the amplitude of the scattering wave vector, **q**, defined as $q = |\mathbf{q}| = (4\pi/\lambda)\sin(\theta/2)$, where λ is the wavelength of the incident beam, θ the scattering angle in medium, and the q_x, q_y and q_z are the respective components of **q**. (b) The typical shear-induced butterfly type SALS pattern at $\dot{\gamma} = 100\ s^{-1}$ observed for a single-phase state of PS/DEM 6.0 wt.% at $T = 50$ °C, which is above the cloud point temperature as indicated by the upper cross symbol in Fig. 1. μ is the azimuthal angle for the scattering pattern.

2.3. Initial condition before shear-jump

The phase-separating structure of PS/DEM as an initial state was prepared by the following way: after installing the solution in the shear cell, it was annealed at 50 °C, which is well above $T_{cl} = 32$ °C, for about 3 h to erase any thermal and shear histories of solutions. The solution was then quenched to 30 °C which is lower than the cloud point by 2 °C. The quench induced the spinodal decomposition (SD), and a periodic phase-separating structure was formed. When the characteristic length of the spinodally decomposed domain structures became about 10 μm, we applied a step-up shear flow to the samples from 0 s^{-1} directly to given shear rates, and then observed further changes in the light scattering patterns and optical microscope images. We shall report our

results obtained at 0.1 and 3.16 s^{-1}, as representative results below and above $\dot{\gamma}_{c,SD}$, respectively.

3. Results

3.1. Effects of a weak shear flow of $\dot{\gamma} = 0.1$ s^{-1} on phase-separating structures

Effects of the shear flow on the phase-separating structures developed via SD in the thermodynamically unstable region, as described in Section 2.3, are explored by means of the real space analysis as also described in Section 2.2. Fig. 3 shows transmission optical micrographs (top halves) and the corresponding two-dimensional fast Fourier transformation (2D-FFT) patterns (bottom halves). In order to examine the characteristic wave number of the dominant Fourier modes of the concentration fluctuations under the flow, we estimated the scattering vector $\mathbf{q}_m$ at the FFT intensity maximum, as demonstrated, for example, in Fig. 4 by arrows. The value of $\mathbf{q}_m$ was determined by best-fitting procedure to the FFT data. The trajectory of $\mathbf{q}_m$ is also drawn as a white dotted line for each FFT pattern in Fig. 3(f)–(j).

Fig. 3(a) shows the microscopic image of the initially phase-separating structure just before imposition of the shear flow ($t = 0$ s). The seemingly bicontinuous phase-separating structure has been formed by the isothermal spinodal decomposition at 30 °C as evidenced by the spinodal ring in the corresponding 2D-FFT pattern in part (f). The spinodal ring is more clearly evidenced by Fig. 6(a), which will be shown later. At $t = 0$ s, the 2D-FFT image is isotropic, and the intensity maximum occurs at $q \cong q_m \simeq 7 \times 10^{-4}$ nm^{-1} independently of azimuthal angle, μ, as shown in Fig. 3(f), where q_m is the magnitude of $\mathbf{q}$ at the maximum intensity. Since the dominant wavelength of Fourier modes of the concentration fluctuations, Λ_m, is given by $\Lambda_m \equiv 2\pi/q_m$, Λ_m is estimated to be $\sim$10 μm at $t = 0$ s.

After the onset of the weak shear flow with $\dot{\gamma} = 0.1$ s^{-1}, the bicontinuous phase-separating structure grows very slowly as shown in Fig. 3(b)–(e). From each corresponding 2D-FFT pattern in parts (g)–(j), the trajectory of $\mathbf{q}_m$ shrinks along q_x with time and gradually becomes an elliptical ring elongated along q_z, indicating that the characteristic length of the deformed domain structure along x increases with time. However, at 100 s, the 2D-FFT pattern is nearly isotropic, and q_m along x and z axes is almost same as that at $t = 0$ s, even though the total strain imposed on the system is as large as $\dot{\gamma}t = 10$. To our big surprise, this indicates that the effect of the shear flow on the deformation of the spinodal ring seems apparently very small. We shall further discuss the observed surprise and our interpretation in Section 4 later. By 600 s, the image contrast increases, so that the pattern consisting dark and bright regions becomes more distinct, and the trajectory of $\mathbf{q}_m$ becomes surely elliptic. The elliptic pattern indicates that the phase-separating structure is elongated along the flow direction with Λ_m parallel to the flow direction (Λ_{mx}) being larger than that perpendicular to the flow direction (Λ_{mz}). We expect that the development of the concentration fluctuations via SD is very slow due to the viscoelastic effects [30,31] as described already in Section 1.

In order to make more quantitative observation, we show the relative intensity distribution of each 2D-FFT image of Fig. 3(f)–(j) in Fig. 4. The peak position, q_m, shifts toward small q with time for both parallel and perpendicular to the flow direction, though q_m parallel to the flow direction, q_{mx}, decreases faster than q_m normal to the flow direction, q_{mz}, as described above. The time dependence of q_{mx} and q_{mz} is shown in Fig. 5. Obviously, phase-separating structure grows very slowly and becomes asymmetric only at about 300 s after the onset of the shear flow. The very slow growth is due to the elastic effects, which is consistent with the earlier reports in the quiescent solutions [30,31].

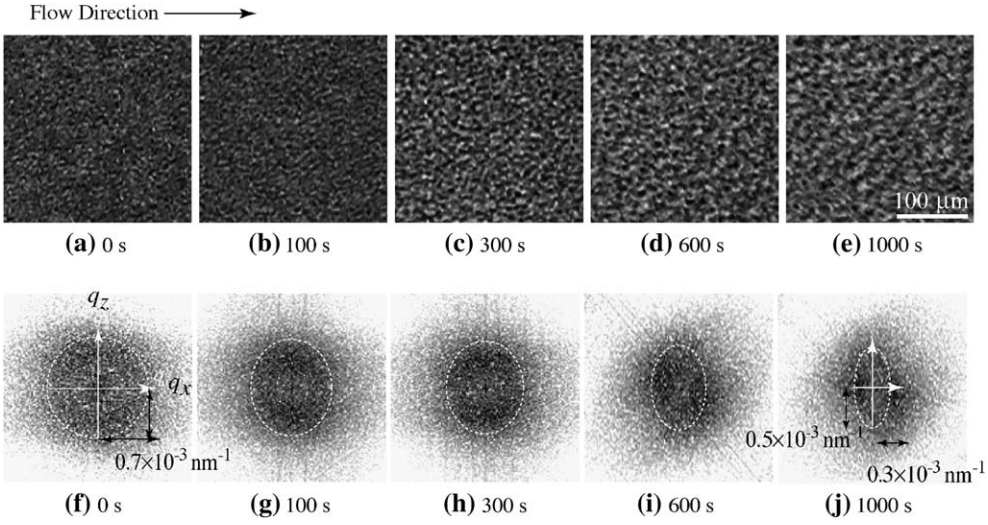

Fig. 3. Transmission optical microscope images, (a)–(e), and their corresponding 2D-FFT images, (f)–(j), of PS/DEM 6.0 wt.% at $\dot{\gamma} = 0.1$ s^{-1} and at 30 °C, which is 2 K below the cloud point temperature. The annotation beneath in each image or pattern indicates the time after which shear flow was imposed on the system. The flow direction (the x axis) is along the horizontal direction.

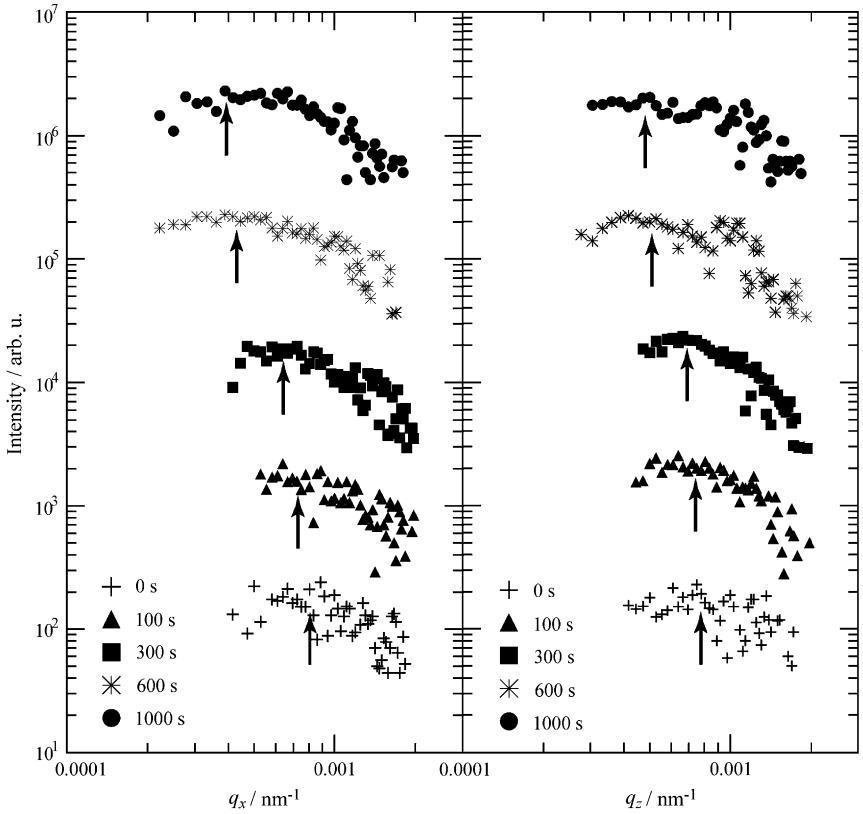

Fig. 4. Time-dependent relative intensity profiles obtained from 2D-FFT images in Fig. 3(f)–(j) along q_x and q_z for PS/DEM 6.0 wt.% at $\dot{\gamma} = 0.1\ s^{-1}$ and at 32 °C. Consecutive intensity profiles have been shifted vertically in order to avoid overlap. The arrows indicate q values at maximum intensity, q_{mx} and q_{mz}, at various times after onset of shear flow.

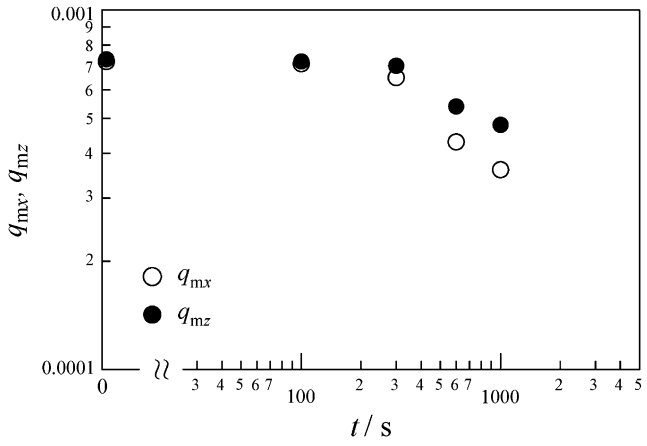

Fig. 5. Time evolution of q_{mx} and q_{mz} as evaluated from Fig. 4(a) and (b), respectively.

3.2. Effects of a strong shear flow of $\dot{\gamma} = 3.16\ s^{-1}$ on phase-separation structures

The simple shear flow of $\dot{\gamma} = 3.16\ s^{-1}$ is imposed on the phase-separating system at $T = 30$ °C. The initial state before applying the flow is almost the same as that of $\dot{\gamma} = 0.1\ s^{-1}$ described in Section 3.1. Before applying the shear flow, the scattering pattern exhibits a "spinodal ring" pattern as shown in Fig. 6(a), which indicates that the phase-separating structure is isotropic. In the time scale from immediately after the onset of the shear flow to the first 1 s (Fig. 6(b)), the ring pattern was kept in the same size as that in Fig. 6(a), although $\dot{\gamma}t$ is already as large as about 3. Then a strong intensity maximum emerges approximately along the q_x and the $-q_x$ directions at $t = 2$ s, while that of along q_z is decreasing with time. This causes butterfly like scattering pattern as shown in Fig. 6(c).

Upon further increasing the time, the intensity along q_x and a spread of the butterfly pattern along μ increase further. At $t = 3$ s after the onset of the shear flow (Fig. 6(e)), the scattering intensity along q_x as well as that along higher μ become even higher and the butterfly expands its wings in the q_x–q_z plane, resulting in sharpening or narrowing of the "*dark streak*" around the q_z axis [4,5]. The intensity increase of the anisotropic pattern indicates that the amplitude of concentration fluctuations is increased in all directions except for the z direction. From Fig. 6(f) ($t = 4$ s), it is clear that the initial spinodal ring-like pattern completely disappeared and is turned over by the butterfly pattern with the strong scattering intensity.

The butterfly-shaped patterns gradually shrink in the q_x–q_z plane, indicating the coarsening of the domains parallel to the flow. The concentration fluctuations perpendicular to the flow, which had a characteristic wavelength, Λ_{mz}, at the initial state, are completely suppressed by the flow. Since the butterfly pattern neither disappears nor changes its own shape during the

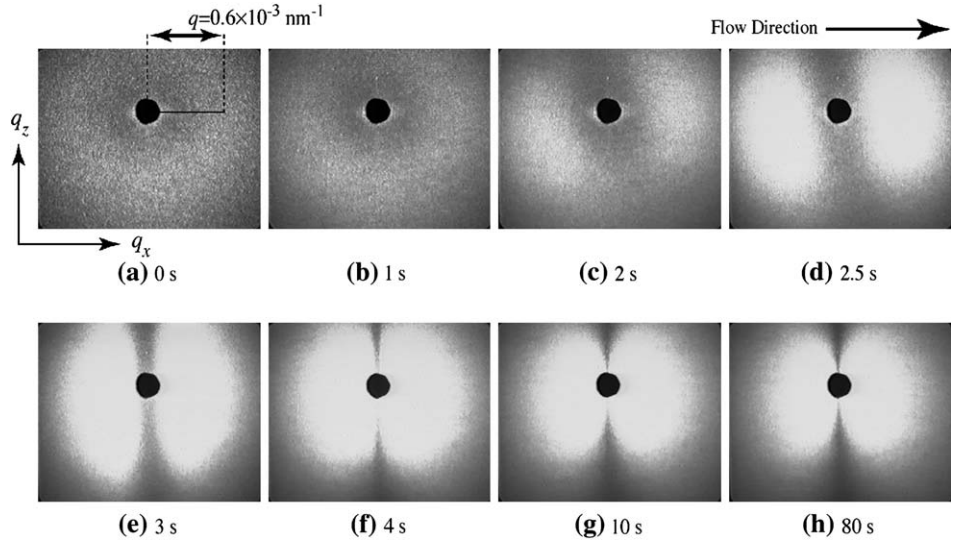

Fig. 6. Time evolution of 2D-SALS patterns for PS/DEM 6.0 wt.% at $\dot{\gamma} = 3.16\ s^{-1}$ and at 30 °C. The characteristic length of concentration fluctuations at the initial state before imposing the shear flow, as evaluated from pattern (a), was ($\Lambda_m \equiv 2\pi/q_m \approx$) 10 ± 2 μm. The annotation beneath each pattern indicates the time after which shear flow was imposed on the system.

presence of the shear flow as shown in Fig. 6(g) and (h), these scattering patterns reflect their steady-state structures formed under the steady shear flow at shear rate of $3.16\ s^{-1}$.

Finally we briefly compare some differences between the butterfly scattering developed in the single-phase solution (Fig. 2(b)) and that in the two-phase solution. Fig. 7 compares the two butterfly patterns in terms of contour plots comprised of a series of iso-intensity lines. The black and red lines, respectively, show the steady-state butterfly in Fig. 2(b) ($\dot{\gamma} = 100\ s^{-1}$ at 50 °C) and that in Fig. 6(h) ($\dot{\gamma} = 3.16\ s^{-1}$ at 32 °C). The two contour patterns shown in Fig. 7 are apparently similar to each other over the q-range covered in the figure, except for a big difference in the intensity level: the intensity level for the pattern in Fig. 6(h) is higher than that in Fig. 2(b) by at least 10 times. The structure created under a shear flow surely depends on the temperature and the shear rate. Nevertheless, the results reveal that the amplitude of concentration fluctuations built-up is larger for the solution in initially two-phase region than that in initially one-phase region. Our explanation will be described afterwards in the context of the HFMO theory.

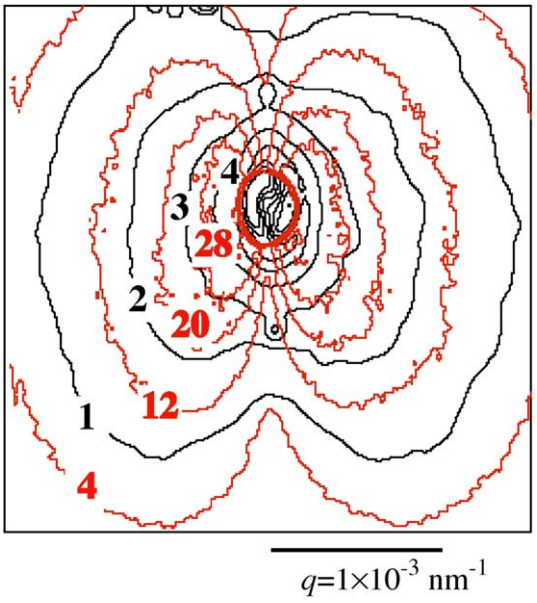

Fig. 7. The contour plots of the steady-state butterfly patterns for PS/DEM 6.0 wt.% at $\dot{\gamma} = 100\ s^{-1}$ and at 50 °C (single-phase region) and at $\dot{\gamma} = 3.16\ s^{-1}$ and at 32 °C (two-phase region). The black and red lines, respectively, indicate the steady-state butterfly in single-phase region and in two-phase region. The numbers indicated on each contour line represent intensity ratio of each line with respect to the intensity of the contour line numbered 1. The relative intensity level for the pattern in red is higher than that in black by at least 10 times.

It should be noted that the similarity of the red and black patterns in Fig. 7 is limited to higher q values: the pattern in black becomes more and more isotropic at low q values, while the pattern in red stays highly anisotropic. This may be primarily due to an artifact arising from the parasitic scattering from incident beam at the low q values. This artifact more strongly affects the net scattering in the low q region in the case of $T = 50$ °C than in the case of $T = 30$ °C, because the parasitic scattering is independent of temperature, while the true scattering at 50 °C is much weaker than that at 30 °C.

4. Discussion

We shall now discuss the strong shear-rate dependence of the dissipative structures formed for systems in the two-phase region in the context of the generalized TDGL equation given by Eq. (1). Since α is not zero for our semidilute solution, the shear flow affects our system through the velocity field and the stress term. In this case, the shear-rate dependence can be divided into two regions at the critical shear rate, $\dot{\gamma}_{c,SD}$.

4.1. Weak shear-flow region ($\dot{\gamma} < \dot{\gamma}_{c,SD}$)

When $\dot{\gamma} < \dot{\gamma}_{c,SD}$, the domains grow, driven by the thermodynamic term, but they are deformed by the velocity field which is coupled with the stress term. Therefore the scattering patterns become elliptic ring. The deformed polymer-rich domains are comprised of deformed swollen-networks of entangled polymer chains, and the stored energy, which is borne only by the polymers, is partially dissipated via the solvent squeeze mechanism under the flow. This is the case for the low shear rate at $\dot{\gamma} = 0.1\ s^{-1}$ in the present study.

The 2D-FFT pattern in Fig. 3(g) and the corresponding data of time-dependent relative intensity distribution in Fig. 4 show almost no deformation of the spinodal ring, despite the fact that the system is subjected to a large shear deformation of $\dot{\gamma}t = 10$. In the case of dynamically symmetric systems where the spinodally decomposed structures are subjected to the shear flow [14,32,33] or shear deformation [34], the scattering patterns at $\dot{\gamma}t = 10$ were found to become an elliptic ring having $q_{mz}/q_{mx} \simeq 10$ [32]. This point will be further clarified later in this section. Thus the small deformation of the elliptic ring in Fig. 3(g) is really an unpredicted surprise to us. We shall present below a possible interpretation on this intriguing result.

The initial phase-separating structures are formed in quiescent state via SD under the strong viscoelastic effects [9,30,31]. Thus the system forms three-dimensionally (3D) continuous domain structures in the solvent matrix with the characteristic wave number q_m or length Λ_m, even though polymer is a minority phase. The continuous networks of the polymer-rich domains (defined as "*domain network*" for the discussion below) are comprised of entangled polymers swollen by the solvent. The value q_m or length Λ_m decreases or increases, respectively, with time driven by the thermodynamic driving force for SD via the solvent squeeze mechanism and under so-called viscoelastic phase separation [30,31].

When the system is brought under the weak shear at $\dot{\gamma} < \dot{\gamma}_{c,SD}$, the domain network is deformed. The deformed network is relaxed from deformation by a partial breakage of the network, as shown in Fig. 8. Fig. 8 schematically presents the domain network rich in polymer as the lines connected into the network in the matrix of solvent. Part (a) schematically represents undeformed domain network with the characteristic length, Λ_m, developed by the viscoelastic phase separation, while part (b) and part (c), respectively, designate deformed domain network with the characteristic lengths, Λ_{mx} and Λ_{mz}, along x and z axes, respectively, and domain network recovered from deformation through a partial breakage of the network. This partial breakage of the domain networks may occur more or less randomly in space. As a consequence of the breakage, the 3D continuous network domain structure may break into grains which contain the domain network structure as their internal structure. The breakage of the 3D continuous domain network into grains may cause relaxation of deformed domain network inside them, so that the spinodal ring becomes isotropic ($q_{mz} \cong q_{mx}$). As a result, flow of the system may occur in between the interstitial regions between the grains. The grains might be recombined into large grains enhanced by flow-enhanced coalescence, which may be considered as a healing or reformation process of the fractured domain network. The grains themselves may be further deformed, which may induce deformation of the internal domain network structure and its partial breakage. These processes, i.e., the deformation of grains and the partial breakage of the internal domain network, may cause a breakage of grains into smaller grains and relaxation of the deformed domain network structure inside grains in turn. The domain network structure inside grains may coarsen via the solvent squeezing process involved by the partial breakage of the domain network and by an incorporation (or welding) of the broken domain networks into a part of the continuous domain network.

The deformation, partial breakage, relaxation, reformation, and growth of the domain networks may be repeated under the weak shear flow, and during this cycle the domain network will grow or coarsen via the viscoelastic phase-separation mechanism. As time elapses, the aspect ratio of the elliptical spinodal ring increases. The percolated networks will be eventually collapsed and transformed into deformed swollen domains comprised of polymers, which are elongated, parallel to the flow direction and which are dispersed in the solvent

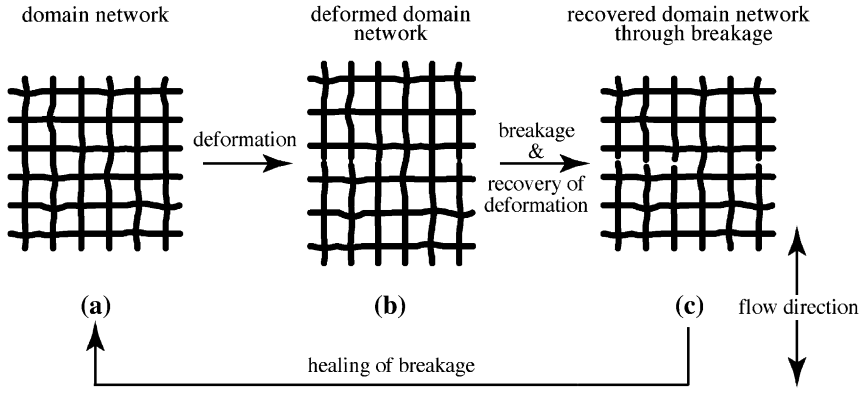

Fig. 8. Schematic illustration to explain small deformation of spinodal ring or spinodally decomposed structure at $\dot{\gamma} < \dot{\gamma}_{c,SD}$. The model is based on a repeated cycle of processes which involve deformation of domain network formed via viscoelastic phase separation (schematically drawn by the thick lines), breakage of the domain network, elastic recovery of the network, and healing of the breakage.

matrix, in the hydrodynamic limit of large spatial and temporal scale; as a consequence the system behaves as a viscous fluid, although this limit was not attained in this work as evidenced by Figs. 3(j) and 5. In the hydrodynamic limit polymer chains inside the domains will be hardly deformed, and stress will be primarily stored via deformation of domain interface as in the case of dynamically symmetric mixtures [9,35].

4.2. Comparison with behavior in dynamically symmetric system

Before going into detailed discussion about the strong shear-flow regime at $\dot{\gamma} > \dot{\gamma}_{c,SD}$, it would be worthwhile to note the corresponding behavior of a dynamically symmetric system. Fig. 9 represents time evolution of light scattering patterns for a dynamically symmetric system. The system studied is a semidilute solution comprised of a mixture of PS and polybutadiene (PB) having composition of 50/50 by weight dissolved in a common solvent of dioctylphthalate (DOP) where the total polymer concentration is 3.3 wt.%. This system designated as PS/PB(50:50)/DOP 3.3 wt.% has cloud point temperature, T_{cl}, at 78 °C, and therefore undergoes the macroscopic phase separation into the following two phases at 74 °C: one phase is PS-rich solution, and the other phase is PB-rich solution, because DOP is neutral solvent for both PS and PB. Further details of the system should be referred to elsewhere [12,14,15,32].

The system was first brought into a single-phase state at 74 °C by raising the shear rate to $\dot{\gamma} = 8.9\ s^{-1}$, which is above the critical shear rate, $\dot{\gamma}_c = 2.5\ s^{-1}$, for the shear-induced single-phase formation (pattern (a) in Fig. 9) [9,11,12]. Then at the same temperature, $\dot{\gamma}$ was abruptly dropped to $0.214\ s^{-1}$, so that SD occurs under the shear flow and hence strong scattering arises from the sheared system, due to the shear deformation of spinodally decomposed structures, as shown by time change in the deformed spinodal patterns in Fig. 9(b)–(d), after the onset of the shear drop. Even at 100 s after the shear drop, i.e., at a small total strain of 21.4, the spinodal ring was remarkably deformed into an ellipsoidal ring highly elongated

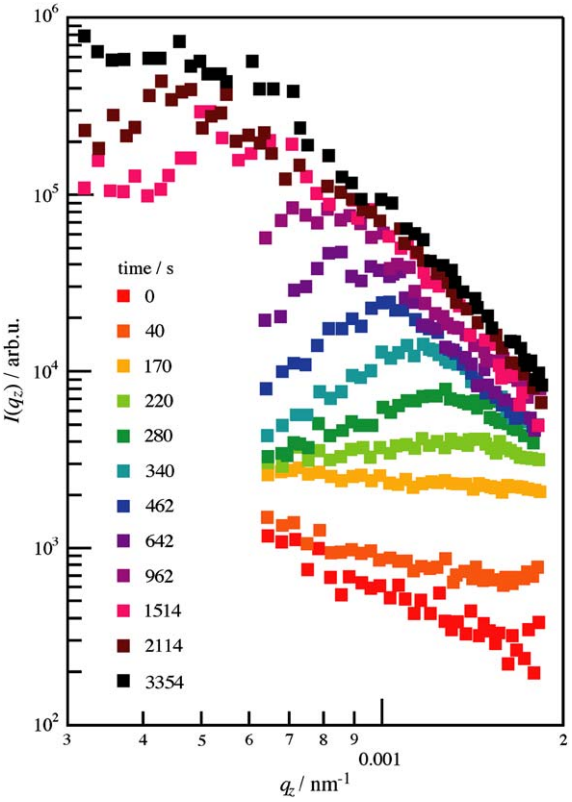

Fig. 10. Scattering intensity distributions along the neutral axis, $I(q_z)$, at various times after the onset of the phase separation under shear flow. The results were observed in the same experiment as that shown in Fig. 9.

along the neutral axis (the q_z direction) and highly compressed along the flow direction (the q_x direction). Upon further increase of time or shear strain, $\dot{\gamma}t$, the scattering patterns are further compressed along q_x, and the scattering intensity further increases, so that the scattering maximum originating from the spinodally decomposed structure appears to be obscured in patterns (c) and (d). However, a quantitative analysis of scattering profile clarifies that the scattering maximum still clearly remains at 220 and 1100 s or even after 2114 s as demonstrated in Fig. 10 for $I(q_z)$. Fig. 10 quantitatively indicates

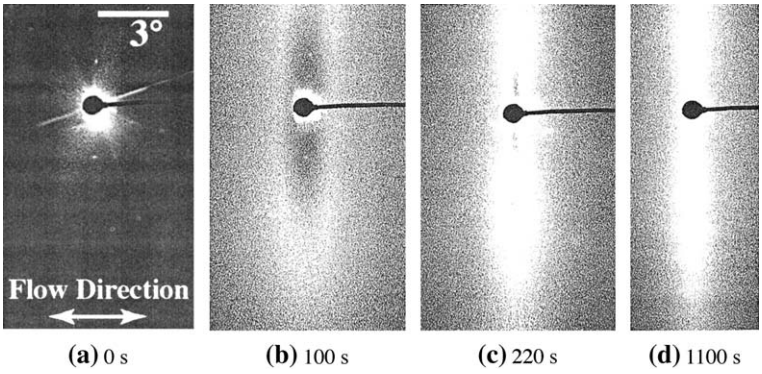

Fig. 9. Time evolution of scattering patterns in $q_x - q_z$ plane after the onset of SD under the shear flow at $\dot{\gamma} = 0.214\ s^{-1}$ for a dynamically symmetric system of PS/PB(50:50)/DOP 3.3 wt.%; (a) 0 s, (b) 100 s, (c) 220 s, and (d) 1100 s after the onset of phase separation under the shear flow. The q_x and q_z directions are parallel to horizontal and vertical directions of the figure, respectively. The pattern (a) at 0 s corresponds to the one from shear-induced single-phase state, and the pattern around the beam stop is still a part of incident beam.

that: (i) scattered intensity along q_z increases and (ii) q_{mz} decreases with time after the shear drop as shown in Fig. 10. The time evolution of q_{mz} and $I(q_z)$ shown in Fig. 10 was discovered to be scaled by the *shear-rate dependent characteristic time and length* [14]. Thus a new concept that shear rate also changes characteristic time and length of the nonequilibrium systems was for the first time elucidated in the literatures.

The above results are interpreted as a consequence of coarsening of the phase-separated domains and also as a consequence of deformation of the domains due to viscous drag. It is to be stressed here that the domain deformation due to the shear flow involved almost no molecular orientation into the system, as evidenced by no observable amount of birefringence in the sheared solution. Consequently, the elastic effects are irrelevant to this system. The comparison of the two systems, PS/PB(50:50)/DOP 3.3 wt.% and PS/DEM 6.0 wt.%, clearly highlights significance of the elastic effects on the phase separation for the latter system.

4.3. Strong shear-flow region ($\dot{\gamma} > \dot{\gamma}_{c,SD}$)

As shear rate further increases above $\dot{\gamma}_{c,SD}$ for our asymmetric system, the stress level also further increases. Therefore the stress term in Eq. (1) becomes dominant over the thermodynamic term and controls the dissipative structures. Since the stress level imposed on the domain networks is high, and the network is subjected to large deformation for a given period of time, as schematically shown in the change from part (a) to part (b) in Fig. 11. Under this condition, the network may be collectively broken into pieces as visualized in part (c). Since parts of the network aligned parallel to flow will be more likely broken than those perpendicular to it, grains of the broken domain network should have a shape extended perpendicular to the flow as shown in part (c). The deformed domain network is recovered from deformation after the breakages of the domain network. However, the breakages may not be healed, on the contrary to the case of $\dot{\gamma} < \dot{\gamma}_{c,SD}$. This may reflect that the deformation rate is larger than the rate of healing or reformation of the domain network via coalescence of the broken domains. The breakages enhance concentration fluctuations along q_x, because they create the regions where the domain networks exist and hence polymer concentration is high and the regions exclusively occupied by solvent. This provides a "solvent squeezing process of the domain network", analogous to the solvent squeezing process of entangled polymer chains in a single-phase solution under shear flow. The solvent squeezing process of entangled polymer chains in the two-phase solution under shear flow occurs when parts of deformed networks themselves are relaxed via the network breakages.

On the contrary to q_x direction, the breakage may have relatively small effects on concentration fluctuations along q_z. These account for the butterfly pattern as shown in Fig. 6(c)–(h), similar to the case of the sheared single-phase solution at $\dot{\gamma} > \dot{\gamma}_{cx}$ (see for example Fig. 21 in Ref. [9]). It should be stressed here, however, that the enhancement of concentration fluctuations for the phase-separated domain systems under flow should be much larger than that for the single-phase solution under shear flow, as evidenced by the results shown in Fig. 7 and as will be discussed later in this section.

Furthermore it should be also noted that centers of mass of the broken domain networks would not be aligned in a line along the flow direction as in the case shown in part (c) which presents our oversimplified model, but they are rather placed more or less randomly along the neutral axis (horizontal axis of the figure). If they are aligned along the flow direction, we should be able to observe a strong streak-like scattering pattern oriented along the neutral direction which is superposed on the butterfly pattern, as in the case of the string-like dissipative structures formed for the sheared single-phase solution at $\dot{\gamma} > \dot{\gamma}_a$ (see Fig. 8 in Refs. [36] and [37]) [9].

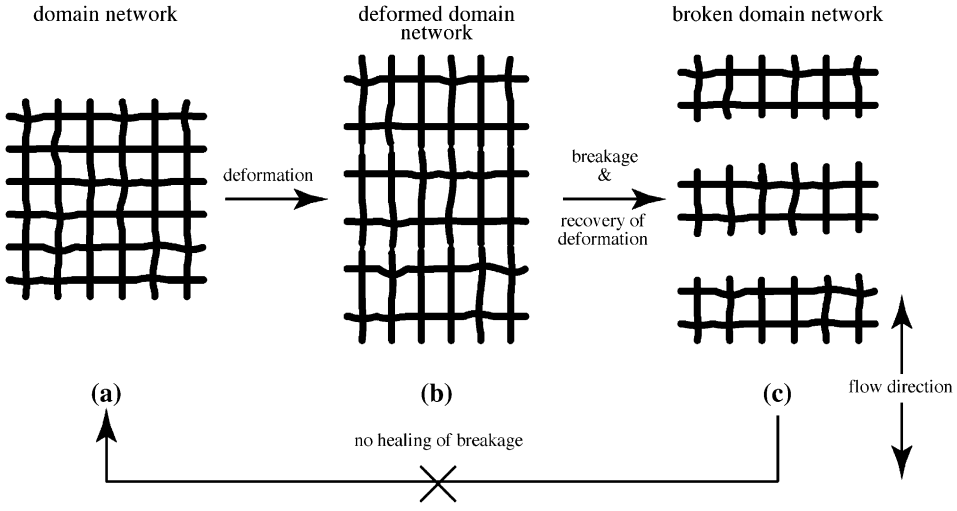

Fig. 11. Schematic illustration to explain butterfly scattering patterns at $\dot{\gamma} > \dot{\gamma}_{c,SD}$. The model is based on a large deformation of domain network formed via viscoelastic phase separation (schematically drawn by the thick lines), collective breakages of parts of the networks oriented parallel to flow, and elastic recovery of the domain network. The broken domains will not be healed into nearly the same original domain network contrary to the case shown in the change from (c) to (a), because of a large deformation rate.

It is crucial to comment some differences between the shear-induced butterfly patterns developed for the single-phase solution in quiescent state and those developed for the two-phase solution in quiescent state, the latter part of which is described above in Section 3.2. The latter butterfly patterns reflect the larger amplitude of concentration fluctuations than the former butterfly patterns at least by about three times, simply because the scattering intensity of the latter is higher than the former by about 10 times. There must be an even more important difference, which is expected to appear in high q region where scattering reflects primarily domain interface and thermal concentration fluctuations within the polymer-rich domains, although we could not attain this q region in this work. We would expect the following for the shear-induced structures for the two-phase solutions in quiescent state: (i) the domain interface must have a sharp boundary so that the scattering intensity, $I(q)$, should obey Porod's law, $I(q) \sim q^{-4}$ and (ii) Ornstein–Zernicke (OZ) type scattering intensity in the polymer-rich domains should be much suppressed compared with that of the corresponding sheared solutions which are in single-phase state in absence of the shear flow, simply because local polymer concentration in the domain is expected to be larger than polymer concentration in the single-phase solution. It should be noted that the domain interface is less well defined for the sheared solution in the single-phase state [38]. This will be best explored by the small-angle neutron scattering coupled with a deuterium labeled technique [38,39].

Last of all, we should notice that the characteristic scattering vector $\mathbf{q}_m$ rotates counterclockwise with respect to the flow direction in the case of $\dot{\gamma} = 3.16\ s^{-1}$ in the time period between 2 and 2.5 s, as shown in Fig. 6(c)–(d). The orientation of the vector $\mathbf{q}_m$ may not be attributed to some physical meaning such as the convection effect of concentration fluctuations in the q_x–q_z plane, but to some external effective flow factors due to the subtle difference of sample thickness [40].

5. Summary

We have investigated the effects of shear flow on the phase-separation processes in dynamically asymmetric systems under the initial conditions where the isotropic and three-dimensionally continuous phase-separating structures are developed via the spinodal decomposition process in the quiescent state. The shear-rate dependence of the phase-separating structure can be divided into two regions at the critical shear rate, $\dot{\gamma}_{c,SD}$.

At $\dot{\gamma} = 0.1\ s^{-1} < \dot{\gamma}_{c,SD}$, the thermodynamic term is dominant over the elastic term for promoting phase separation. However, the growing phase-separating structures were deformed along the shear direction and consequently the scattering patterns became an elliptic ring shape extended along q_z direction. The viscoelastic effects intrinsic to the dynamically asymmetric systems come into play even in this low shear-rate condition, making the deformation of the elliptic spinodal ring anomalously small, because of the repeated elastic deformation, partial breakage, relaxation, reformation, and coarsening of the domain network as detailed in Section 4.1.

In the case of the shear flow at $\dot{\gamma} = 3.16\ s^{-1} > \dot{\gamma}_{c,SD}$, the scattering pattern changes from the nearly isotropic spinodal ring to the so-called butterfly pattern. This indicates that the stress term dominates the thermodynamic term for promoting phase separation. The detailed processes for the shear-induced butterfly pattern formation and differences in the butterfly pattern formed in the case of $\dot{\gamma} > \dot{\gamma}_{c,SD}$ for the two-phase state and that formed in the case of $\dot{\gamma} > \dot{\gamma}_c$ for the single-phase state were discussed in Section 4.2.

References

[1] ver Strate G, Philippoff WJ. J Polym Sci Polym Lett Ed 1974;12:267.
[2] Rangel-Nafaile C, Metzner AB, Wissbrum KF. Macromolecules 1984; 17:1187.
[3] Wu X-L, Pine DJ, Dixon PK. Phys Rev Lett 1991;66:2408.
[4] Hashimoto T, Fujioka K. J Phys Soc Jpn 1991;60:356.
[5] Hashimoto T, Kume T. J Phys Soc Jpn 1992;61:1839.
[6] Saito S, Matsuzaka K, Hashimoto T. Macromolecules 1999;32:4879.
[7] Endoh MK, Saito S, Hashimoto T. Macromolecules 2002;35:7692.
[8] Imaeda T, Furukawa A, Onuki A. Phys Rev E; 2004:70. 051503.
[9] Hashimoto T. Bull Chem Soc Jpn 2005;78:1.
[10] Beysens D, Gbadamassi M, Boyer L. Phys Rev Lett 1979;43:1253.
[11] Hashimoto T, Takebe T, Suehiro S. J Chem Phys 1988;88:5874.
[12] Takebe T, Sawaoka R, Hashimoto T. J Chem Phys 1989;91:4369.
[13] Hindawi IA, Higgins JS, Galambos AF, Weiss RA. Macromolecules 1990;23:670.
[14] Hashimoto T, Takebe T, Asakawa K. Physica A 1993;194:338.
[15] Hashimoto T, Matsuzaka K, Moses E, Onuki A. Phys Rev Lett 1995;74:126.
[16] Yu J-W, Douglas JF, Hobbie EK, Kim S, Han CC. Phys Rev Lett 1997; 78:2664.
[17] Onuki A. Phase transition dynamics. Cambridge: Cambridge University Press; 2002.
[18] Hohenberg PC, Halperin BI. Rev Mod Phys 1977;49:435.
[19] Hashimoto T, Takebe T, Fujioka K. Nishinomiya-Yukawa symposium on theoretical physics. In: Dynamics and patterns in complex fluids. Heidelberg: Springer; 1989.
[20] Saito S, Koizumi S, Matsuzaka K, Suehiro S, Hashimoto T. Macromolecules 2000;33:2153.
[21] Saito S, Hashimoto T. J Chem Phys 2001;114:10531.
[22] Takenaka M, Miyazawa M, Nishitsuji S, Hashimoto T. J Chem Phys 2004;21:7501.
[23] Helfand E, Fredrickson GH. Phys Rev Lett 1989;62:2468.
[24] Milner ST. Phys Rev E 1993;48:3674.
[25] Onuki A. J Phys Condens Matter 1997;9:6119.
[26] Onuki A, Taniguchi T. J Chem Phys 1997;106:5761.
[27] Kawasaki K, Ohta T. Prog Theor Phys 1978;59:362.
[28] Saito S, Takenaka M, Toyoda N, Hashimoto T. Macromolecules 2001;34: 6461.
[29] Kume T, Asakawa K, Moses E, Matsuzaka K, Hashimoto T. Acta Polym 1995;46:79.
[30] Tanaka H. Macromolecules 1992;25:6377.
[31] Toyoda N, Takenaka M, Saito S, Hashimoto T. Polymer 2001;42:9193.
[32] Takebe T, Hashimoto T. Polym Commun 1988;29:261.
[33] Matsuzaka K, Jinnai H, Koga T, Hashimoto T. Macromolecules 1997;30: 1146.
[34] Izumitani T, Hashimoto T. ACS Symp Ser 1995;597:122.
[35] Hashimoto T. Light scattering from multicomponent polymer systems in shear fields: real-time and in-situ studies of dissipative structures in open-nonequilibrium systems. In: Pecora R, Borsali R, editors. Soft matter: scattering, imaging and manipulation, vol. II. Kluwer [chapter 4], in press.
[36] Kume T, Hashimoto T. ACS Symp Ser 1995;597:122.
[37] Kume T, Hashimoto T, Takahashi T, Fuller GG. Macromolecules 1997; 30:7232.

[38] Saito S, Hashimoto T, Morfin I, Linder P, Boué F, Pine DJ. Macromolecules 2003;36:3745.
[39] Saito S, Hashimoto T, Morfin I, Linder P, Boué F. Macromolecules 2002; 35:445.
[40] This rotation is due to the orientation of domains by shear flow. However, the clockwise rotation should also exist, since the initial state is the isotropic phase-separating structure. Namely, the probability of having the orientation of concentration fluctuations toward clockwise or counterclockwise should be equal. A possible source to rotate the scattering patterns counterclockwise with respect to the flow direction may be attributed to the minor flow along the radial direction of the shear cell from its center to periphery due to centrifugal force in the beginning of the onset of shear flow.